

Comparison of highly-compressed $C2/m$ -SnH₁₂ superhydride with conventional superconductors

E. F. Talantsev^{1,2*}

¹M.N. Mikheev Institute of Metal Physics, Ural Branch, Russian Academy of Sciences,
18, S. Kovalevskoy St., Ekaterinburg, 620108, Russia

²NANOTECH Centre, Ural Federal University, 19 Mira St., Ekaterinburg, 620002,
Russia

*E-mail: evgeny.talantsev@imp.uran.ru

Abstract

Satterthwaite and Toepke (1970 *Phys. Rev. Lett.* **25** 741) predicted high-temperature superconductivity in hydrogen-rich metallic alloys, based on an idea that these compounds should exhibit high Debye frequency of the proton lattice, which boosts the superconducting transition temperature, T_c . The idea has got full confirmation more than four decades later when Drozdov *et al* (2015 *Nature* **525** 73) experimentally discovered near-room-temperature superconductivity in highly-compressed sulphur superhydride, H₃S. To date, more than a dozen of high-temperature hydrogen-rich superconducting phases in Ba-H, Pr-H, P-H, Pt-H, Ce-H, Th-H, S-H, Y-H, La-H, and (La,Y)-H systems have been synthesized and, recently, Hong *et al* (2021 *arXiv:2101.02846*) reported on the discovery of $C2/m$ -SnH₁₂ phase with superconducting transition temperature of $T_c \sim 70$ K. Here we analyse the magnetoresistance data, $R(T,B)$, of $C2/m$ -SnH₁₂ phase and report that this superhydride exhibits the ground state superconducting gap of $\Delta(0) = 9.2 \pm 0.5$ meV, the ratio of $2\Delta(0)/k_B T_c = 3.3 \pm 0.2$, and $0.010 < T_c/T_F < 0.014$ (where T_F is the Fermi temperature) and, thus, $C2/m$ -SnH₁₂ falls into unconventional superconductors band in the Uemura plot.

Comparison of highly-compressed $C2/m$ - SnH_{12} superhydride with conventional superconductors

I. Introduction

Satterthwaite and Toepke [1] were first who understood that hydrogen-rich compound should exhibit highest superconducting transition temperature: "...There has been theoretical speculation [2] that metallic hydrogen might be a high-temperature superconductor, in part because of the very high Debye frequency of the proton lattice. With high concentrations of hydrogen in the metal hydrides one would expect lattice modes of high frequency and if there exists an attractive pairing interaction one might expect to find high-temperature superconductivity in these systems also." Mathematical rigorous description of Satterthwaite's and Toepke's idea [1] had been given 34 years later by Ashcroft [3].

In 2015 Drozdov *et al* [4] reported on experimental discovery of first near-room-temperature superconductor (NRTS) H_3S , which was also the first superhydride compound synthesized at megabar pressure level heated by laser pulses inside of diamond anvil cell. This technique is used since then to synthesize new NRTS phases, and to date more than a dozen high-temperature hydrogen-rich superconducting phases have been synthesised in Pr-H [5], Ba-H [6], P-H [7], Pt-H [8], Ce-H [9], Th-H [10,11], S-H [4,12-17], Y-H [18,19], La-H [20-24], (La,Y)-H [25] and CaH_x [26,27] systems.

Recently, Hong *et al* [28] extended superhydride family by the discovery of $C2/m$ - SnH_{12} phase which exhibits the superconducting transition temperature of $T_c \sim 70$ K at pressure of $P = 190$ GPa. This experimental result is in a good accord with first-principles calculations performed in 2015 by Esfahani *et al* [29], who predicted $T_c = 83$ -93 K for $C2/m$ - SnH_{12} phase compressed at pressure of $P = 250$ GPa. Despite Esfahani *et al* [29] predicted that $C2/m$ - SnH_{12} phase can be thermodynamically stable at $P \geq 250$ GPa, XRD studies [28] show that $C2/m$ - SnH_{12} phase is dominant at lower pressure range of $P \sim 200$ GPa. This difference can

be explained by an atomic disorder, hydrogen non-stoichiometry, etc., which are always (in some degree) real world samples features. It should be noted, that here we assume that calculated values for the electron-phonon coupling constant, $\lambda_{e-ph} = 1.25$, and logarithmic average phonon frequency, $\hbar \cdot \omega_{log} = 991 \text{ K}$, reported by Esfahani *et al* [29] for $C2/m\text{-SnH}_{12}$ compressed at $P = 250 \text{ GPa}$ will be still valid for sample compressed at $P = 190 \text{ GPa}$ [28].

Hong *et al* [28] measured magnetoresistance curves, $R(T,B)$, up to applied magnetic field of $B_{appl} = 7 \text{ T}$, from which, by applying analytical equation proposed by Jones *et al* [30]:

$$B_{c2}(T) = \frac{\phi_0}{2 \cdot \pi \cdot \xi^2(0)} \cdot \left(\frac{1 - \left(\frac{T}{T_c}\right)^2}{1 + \left(\frac{T}{T_c}\right)^2} \right) \quad (1)$$

where $\phi_0 = \frac{h}{2 \cdot e}$ is superconducting flux quantum, and $\xi(0)$ is the ground state coherence length, the ground state upper critical field was deduced as $B_{c2}(0) = 11.2 \text{ T}$.

Here we perform further analysis of $R(T,B)$ data reported by Hong *et al* [28] with the purpose to extract the ground state amplitude of the superconducting energy gap, $\Delta(0)$, one of primary parameters of the superconducting state. In addition, we calculate the ratio of transition temperature to the Fermi temperature, T_F , to locate $C2/m\text{-SnH}_{12}$ phase in Uemura plot [31,32].

II. $R(T,B)$ analysis

Primary task in the analysis of $R(T,B)$ data is to deduce the superconducting critical temperature, T_c , for which we recently proposed [33] to use a fit of experimental $R(T,B)$ data to a function:

$$R(T, B_{appl}) = R_0 + k \cdot T + \theta(T_c^{onset} - T) \cdot \left(\frac{R_{norm}}{\left(I_0 \left(F \cdot \left(1 - \frac{T}{T_c^{onset}} \right)^{3/2} \right) \right)^2} \right) +$$

$$\theta(T - T_c^{onset}) \cdot (R_{norm} + (k - k_1) \cdot T_c^{onset} + k_1 \cdot T) \quad (2)$$

where $R_0, R_{norm}, T_c^{onset}, k, k_1,$ and F are free-fitting parameters, and $\theta(x)$ is the Heaviside function.

The first two terms in the Eq. 2, i.e. $(R_0 + k \cdot T)$, are introduced in Ref. 33 to adopt possible ohmic resistance in $R(T,B)$ curve which appears as a result of metallic weak-links in NRTS sample in diamond anvil cell.

The third fitting term in Eq. 2 which approximates the superconducting transition:

$$R(T, B_{appl}) = \frac{R_{norm}}{\left(I_0 \left(F \cdot \left(1 - \frac{T}{T_c^{onset}} \right)^{3/2} \right) \right)^2} \quad (3)$$

was proposed by Tinkham [34] to fit experimental $R(T,B)$ curves in HTS cuprate ceramics, where Tinkham [34] proposed to use:

$$F = \frac{C}{2 \cdot B_{appl}} \quad (4)$$

where C is free-fitting parameter having unit of Tesla, and B_{appl} is applied magnetic field.

Physical background of Eq. 3 was explained by Tinkham [34] as: “ ... *the specific predicted $B^{3/2}$ dependence fits quite well with a variety of published data We also point out that the result ... would hold even if the functional form (which is in our case Eqs. 3,4) were replaced by some other similar function of $U_0/k_B T$, so long as the form of (which is our Eq. 7) holds.*”

In this explanation, Tinkham [34] mentioned the ratio $U_0/k_B T$, where k_B is the Boltzmann constant, and U_0 is a magnetic flux creep activation energy:

$$U_0 = \beta \cdot B_c^2 \frac{\phi_0 \cdot \xi}{\mu_0 \cdot B_{appl}} \quad (5)$$

where, β is (presumed ~ 1) a constant which absorbed all numerical factors, ξ is superconducting coherence length, B_{appl} is applied magnetic field, and B_c is the thermodynamic field:

$$B_c = \frac{\phi_0}{2 \cdot \sqrt{2} \cdot \pi \cdot \lambda \cdot \xi} \quad (6)$$

where λ is the London penetration depth. After further consideration, Tinkham [34] reported, that:

$$\frac{U_0}{k_B \cdot T} = \frac{A}{B_{appl}} \cdot \left(1 - \frac{T}{T_c^{onset}}\right)^{3/2} \quad (7)$$

where A is a constant of Tesla unit. Thus, in overall, Eq. 3 can be considered as a good approximation for the Abrikosov vortex flux creep. However, as it is mentioned by Tinkham [34], there are no restrictions to use other fitting functions which approximate $U_0/k_B T$ term in given superconductor.

As we discussed in previous paper [31], there is a significant disadvantage of Eq. 7, which remains in recent proposal for parameter F given by Hirsch and Marsiglio [35]:

$$F = \frac{1}{2 \cdot \frac{B_{appl}}{B_{c2}(0)}} \quad (8)$$

that Eq. 3 cannot be used to fit $R(T, B_{appl} = 0)$ data, because the division by zero is prohibited. However, it was pointed out in Ref. 33, that there is no necessity for explicit use of B_{appl} in the expression for parameter F , because B_{appl} is known from experiment. Based on this, F can be free-fitting unitless value, which describe the sharpness of the transition.

However, it should be stressed that as it was mentioned by Tinkham [34] that: “...*some other similar function* ...” can be used as well. And based on this, particular deduced F values

are linked to main fitting term of $\left(I_0 \left(F \cdot \left(1 - \frac{T}{T_c^{onset}}\right)^{3/2}\right)\right)^{-2}$ and as far as the goodness of fit is high, the fit will be in use to deduce T_c^{onset} and T_c within established strict mathematical routine, while particular F value has no practical use.

The fourth fitting term in Eq. 2, i.e. $(R_{norm} + (k - k_1) \cdot T_c^{onset} + k_1 \cdot T)$, represents a linear rise in the $R(T, B)$ curve above the onset transition temperature, T_c^{onset} . More details about different terms in Eq. 2 can be found in Ref. 33.

Thus, if $R(T,B)$ fit to Eq. 2 has converged, T_c can be defined at any $\frac{R(T)}{R(T_c^{onset})}$ criterion, for

which in this work we used the $T_{c,0.05}$ criterion:

$$\frac{R(T)}{R(T_c^{onset})} = 0.05 \quad (9)$$

Primary reasons why the superconducting critical temperature for highly-compressed superconductors should be defined at as low as practically possible $\frac{R(T)}{R(T_c^{onset})}$ ratio were discussed elsewhere [36]. Here we only point out that the use of T_c^{onset} criterion, which utilizes in some, but not in all, reports on highly-compressed superconductors, can be objected by experimental fact that the change in $R(T)$ slope, or even sharp drop in $R(T)$, is observable at many phase transitions in condensed matter when structural phase transitions occur [37-39]. Classical example for this is the change in $R(T)$ slope at structural phase transitions α - γ and γ - ϵ in iron [40,41].

In addition to several fits for NRTS materials, which we showed in our previous work [33], in Fig. 1 we fit $R(T,B=0)$ data for $Fm-3m$ -LaH₁₀ phase ($P = 138$ GPa) for which experimental data has been recently reported by Sun *et al* [26]. The fit has high quality (with goodness of fit $R = 0.9981$) and deduced T_c^{onset} and $T_{c,0.05}$ are indicated in Fig. 1.

All fits presented in the manuscript have been performed by utilizing the Levenberg-Marquardt approach in non-linear fitting package of the Origin2017 software.

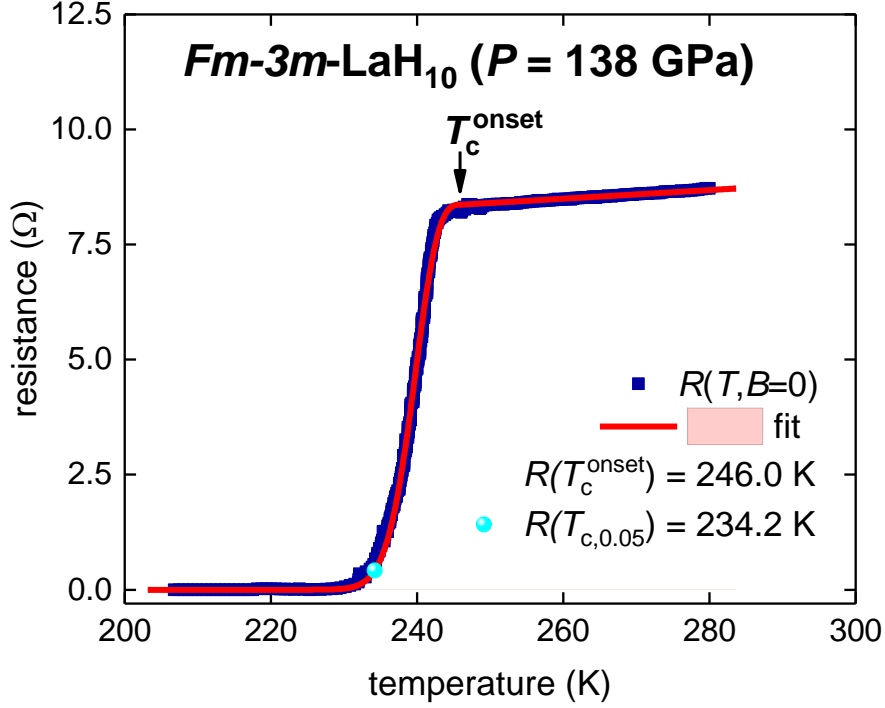


Figure 1. $R(T, B=0)$ data and fit to Eq. 1 for $Fm-3m-LaH_{10}$ ($P = 138$ GPa), where raw data was reported by Sun *et al* [24]. 95% confidence bars are shown by a pink shaded area; goodness of fit is $R = 0.9981$.

III. Results

Fits to Eq. 2 of $R(T, B)$ data for $C2/m-SnH_{12}$ ($P = 190$ GPa) reported by Hong *et al* [28] are shown in Figs. 2,3, where Fig. 2 represents measurements performed at the “cooling” stage, while in Fig. 3 data and fits are shown for the “warming” stage. Despite a fact that $R(T, B)$ curves of $C2/m-SnH_{12}$ ($P = 190$ GPa) phase for “cooling” and “warming” stages are close to each other, these curves are not identical. For this reason, we deduce $T_{c,0.05}(B)$ for each stage with the purpose that full $B_{c2}(T)$ dataset will characterize as complete as practically possible the $C2/m-SnH_{12}$ phase. Results of the analysis are shown in Table 1.

It should be noted that $R(T, B)$ data for $C2/m-SnH_{12}$ ($P = 190$ GPa) reported by Hong *et al* [28] have linear ohmic term below transition temperature, which reflects the presence of metallic weak-links in the sample, which is accounted (as this mentioned above) by the term of $(R_0 + k \cdot T)$ in Eq. 2.

Table 1. Deduced $T_{c,0.05}(B)$ values for the “cooling” and the “warming” stages of $C2/m$ - SnH_{12} phase compressed at $P = 190$ GPa.

Applied field, B_{appl} (Tesla)	$T_{c,0.05}$ (cooling stage) (K)	$T_{c,0.05}$ (warming stage) (K)
0	63.5	65.1
1	57.9	58.6
2	52.4	53.3
3	47.2	48.2
5	35.9	36.4
7	24.8	25.0

In overall, all fits have high-quality, even for $R(T, B=0)$ (Figs. 2,a and 3,a) for which the double transition is observed. For the latter the goodness of fit, $R = 0.9986$, while for the rest $R > 0.9989$.

It should be clarified, that as far as we have defined the critical temperature, T_c , by the $\frac{R(T)}{R(T_c^{\text{onset}})} = 0.05$ criterion (Eq. 9 and Table I), there is no any longer a need to write full designation, i.e. $T_{c,0.05}$, for this value because otherwise there will be a need to use the same subscript for other parameters, i.e. $B_{c2,0.05}(T)$, $\xi_{0.05}(0)$, $\Delta_{0.05}(0)$, etc.. Thus, in further analysis we omit the use of 0.05 designation in the subscripts, because when (which is implemented in many reports) T_c and $B_{c2}(T)$ are defined by 50% of normal state resistance criterion, the designation of used criterion, i.e. $T_{c,0.50}$ and $B_{c2,0.50}(T)$, is always omitted (see, for instance, Ref. 28 where the latter criterion was used).

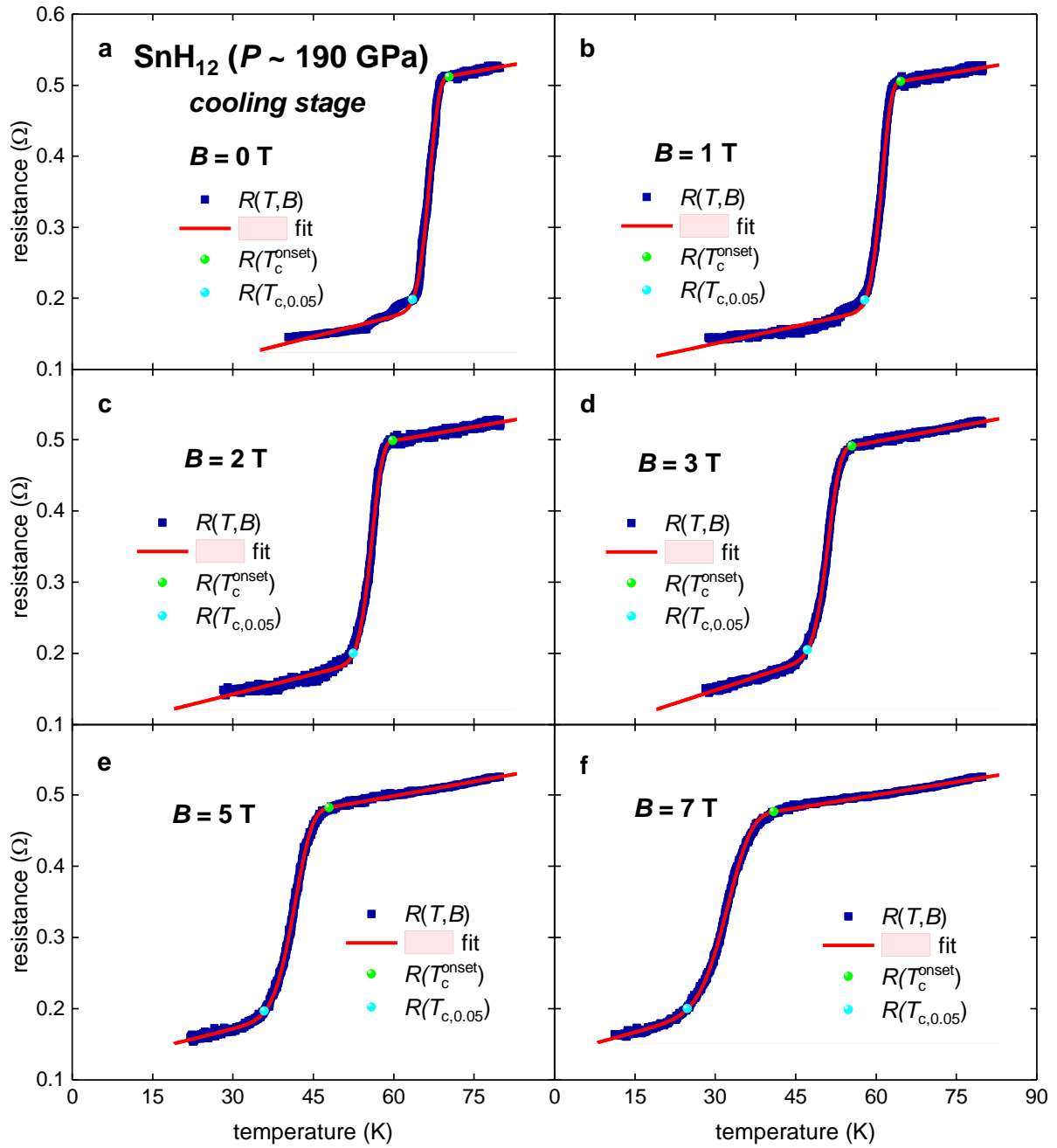


Figure 2. $R(T, B)$ data and fits to Eq. 1 for $C2/m$ - SnH_{12} ($P = 190$ GPa) measured at cooling stage (raw data reported by Hong *et al* [26]). Goodness of fit is: (a) 0.9985, (b) 0.9990; (c) 0.9993; (d) 0.9996; (e) 0.9996; (f) 0.9996.

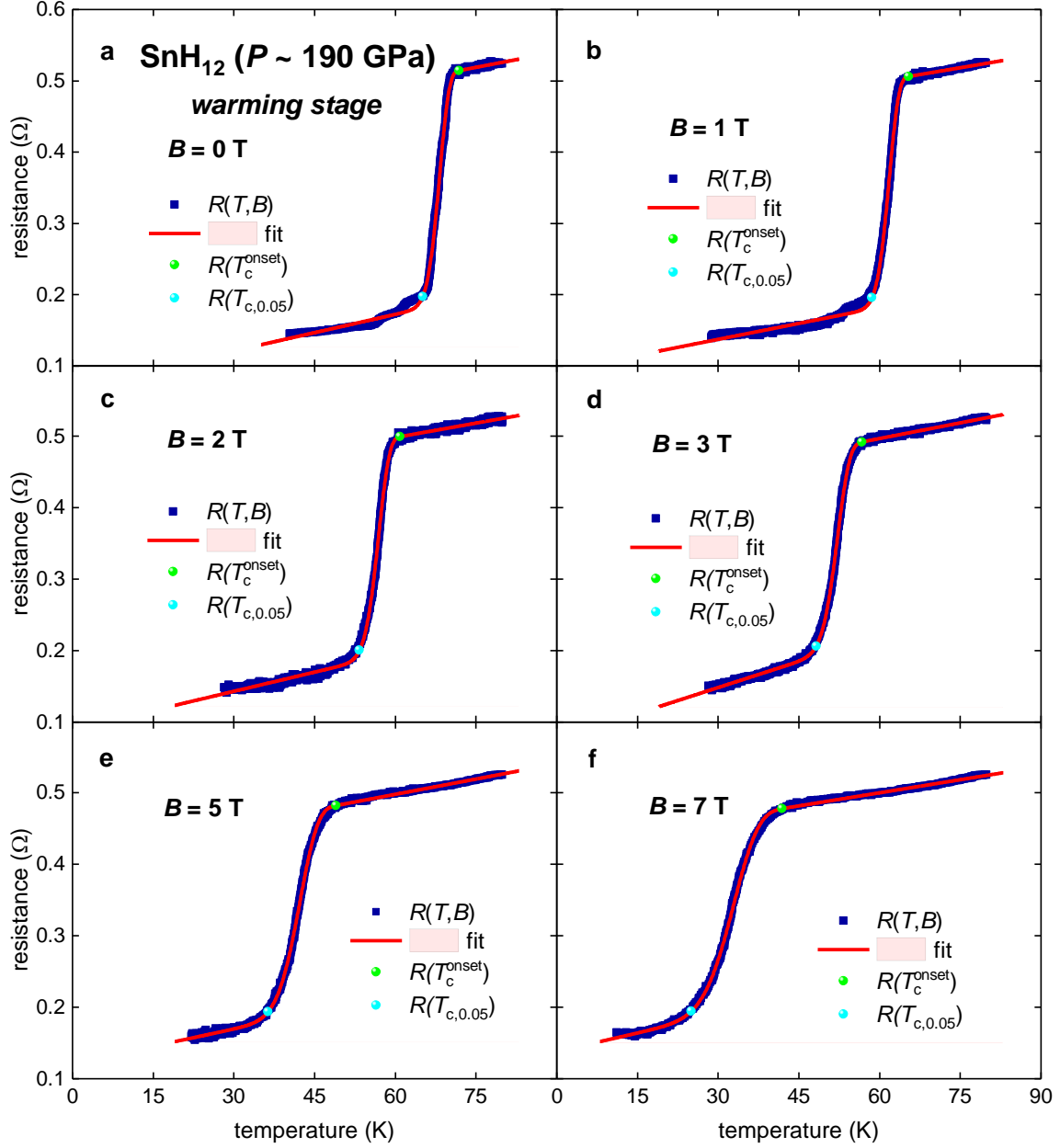


Figure 3. $R(T,B)$ data and fits to Eq. 1 for $C2/m$ - SnH_{12} ($P = 190$ GPa) measured at *warming* stage (raw data reported by Hong *et al* [28]). Goodness of fit is: (a) 0.9987, (b) 0.9990; (c) 0.9992; (d) 0.9996; (e) 0.9996; (f) 0.9996..

Deduced $T_c(B)$ values were used as raw $B_{c2}(T)$ data, which were fitted to upper critical field s -wave model [42]:

$$B_{c2}(T) = \frac{\phi_0}{2 \cdot \pi \cdot \xi^2(0)} \cdot \left(\frac{1.77 - 0.43 \cdot \left(\frac{T}{T_c}\right)^2 + 0.07 \cdot \left(\frac{T}{T_c}\right)^4}{1.77} \right)^2 \cdot \left[1 - \frac{1}{2 \cdot k_B \cdot T} \cdot \int_0^\infty \frac{d\varepsilon}{\cosh^2\left(\frac{\sqrt{\varepsilon^2 + \Delta^2(T)}}{2 \cdot k_B \cdot T}\right)} \right] \quad (10)$$

where k_B is the Boltzmann constant, and the amplitude of temperature dependent superconducting gap, $\Delta(T)$, is given by [43,44]:

$$\Delta(T) = \Delta(0) \cdot \tanh \left[\frac{\pi \cdot k_B \cdot T_c}{\Delta(0)} \cdot \sqrt{\eta \cdot \frac{\Delta C}{C} \cdot \left(\frac{T_c}{T} - 1 \right)} \right] \quad (11)$$

where $\Delta C/C$ is the relative jump in electronic specific heat at T_c , and $\eta = 2/3$ for s -wave superconductors.

Eqs. 10,11 were used to extract $\xi(0)$, $\Delta(0)$, T_c and $\frac{\Delta C}{C}$ in a variety of superconductors, for instance, in highly-compressed H_3S [42], magic-angle twisted bilayer graphene [46], V_3Si [47], $Nd_{0.8}Sr_{0.2}NiO_2$ [48] and iron-based superconductors [47]. Here we applied these equations to extract $\xi(0)$, $\Delta(0)$ and $\frac{2 \cdot \Delta(0)}{k_B \cdot T_c}$ in $C2/m$ - SnH_{12} ($P = 190$ GPa).

Eqs. 10,11 have four-free fitting parameters, $\xi(0)$, $\Delta(0)$, T_c , and $\Delta C/C$, i.e. the same number as one in the standard fitting function for the pinning force density, $F_p(B_{appl})$, [48-51]:

$$F_p(B_{appl}) = F_{p,max} \cdot \left(\frac{B_{appl}}{B_{c2}} \right)^p \cdot \left(1 - \frac{B_{appl}}{B_{c2}} \right)^q \quad (12)$$

where $F_{p,max}$, B_{c2} , p and q are free-fitting parameters. Thus, Eqs. 9,10 can be characterized as a conventional mathematical tool in terms of the number of free-fitting parameters, where each deduced parameter has clear physical meaning.

It needs to be pointed out that $R(T,B)$ curves were measured at only six B_{appl} values, i.e. $B_{appl} = 0, 1, 2, 3, 5, 7$ T, which implies that conventional $B_{c2}(T)$ fit to Eqs. 10,11, where all four parameters are free, needs to be adopted for given $B_{c2}(T)$ dataset (it should be noted that usually [42,47] $B_{c2}(T)$ datasets have up to 30 raw upper critical field data). Thus, there is a need to reduce the number of free-fitting parameters in Eqs. 10,11. We used to fix $\frac{\Delta C}{C}$ value in our previous works [52-54] when experiments were performed over either a narrow temperature range, either at limited set of temperatures. Thus, we assumed that the relative

jump in electronic specific heat at T_c is equal to the Bardeen-Cooper-Schrieffer theory weak-coupling limit for s -wave superconductors [43,44,55,56]:

$$\frac{\Delta C}{C} = 1.43. \quad (13)$$

That left in this case just T_c , $\xi(0)$ and $\Delta(0)$ as free fitting parameters in Eqs. 10,11. $B_{c2}(T)$ data fit to the restricted Eqs. 10,11 is shown in Fig. 4, where it can be seen that the fit has narrow 95% uncertainty bands and deduced parameters are $T_c = 64.6 \pm 0.3 \text{ K}$, $\xi(0) = 6.3 \pm 0.1 \text{ nm}$, $\Delta(0) = 9.15 \pm 0.51 \text{ meV}$, and

$$\frac{2 \cdot \Delta(0)}{k_B \cdot T_c} = 3.28 \pm 0.18. \quad (14)$$

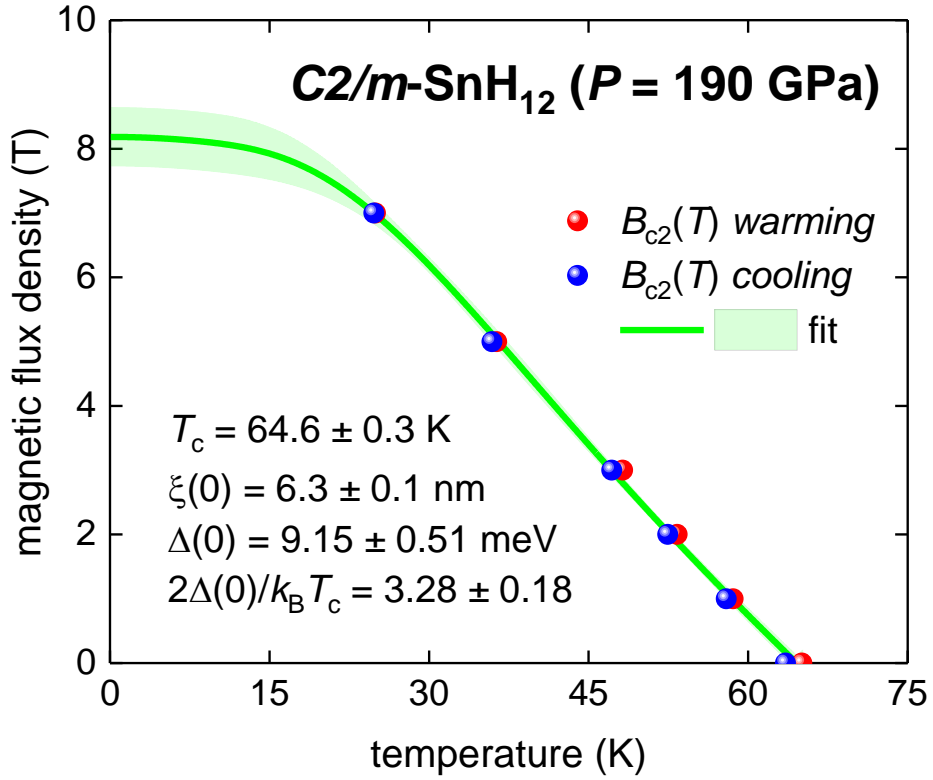


Figure 4. The upper critical field data, $B_{c2}(T)$, and data fit to Eqs. 3,4 for $C2/m$ -SnH₁₂ ($P = 190 \text{ GPa}$). $\frac{\Delta C}{C}$ was fixed to BCS weak-coupling limit of 1.43. 95% confidence bars are shown by a green shaded area; fit quality is $R = 0.9983$.

IV. Comparison of $C2/m\text{-SnH}_{12}$ with conventional superconductors

It might be appeared to be strange that deduced ratio of the gap amplitude to the transition temperature $\frac{2\cdot\Delta(0)}{k_B\cdot T_c} = 3.28 \pm 0.18$ is lower than s -wave BCS weak coupling limit of [43,44,55,56]:

$$\frac{2\cdot\Delta(0)}{k_B\cdot T_c} = 3.53 \quad (15)$$

However, if we assume that $C2/m\text{-SnH}_{12}$ ($P = 190$ GPa) has the Coulomb pseudopotential parameter, $\mu^* = 0.13$, which is weighted average value within many first principle calculations of NRTS materials (where $\mu^* = 0.10\text{-}0.16$ [5,6,9,10,18,25,29,57-71]), and, what is more important, that $\mu^* = 0.13$ was one of probable values used by Esfahani *et al* [29] in their predictive calculations for $C2/m\text{-SnH}_{12}$ phase, than the ratio of $\frac{k_B\cdot T_c}{\hbar\cdot\omega_{ln}}$ has got a value:

$$\frac{k_B\cdot T_c}{\hbar\cdot\omega_{ln}} = \frac{83}{991} = 0.0838. \quad (16)$$

where $\hbar = \frac{h}{2\cdot\pi}$ is the reduced Planck constant, and $\omega_{ln} = \exp\left[\frac{\int_0^{\infty} \frac{\ln(\omega)}{\omega} \cdot F(\omega) \cdot d\omega}{\int_0^{\infty} \frac{1}{\omega} \cdot F(\omega) \cdot d\omega}\right]$, where $F(\omega)$ is the phonon density of states.

In result, the plot of $\frac{2\cdot\Delta(0)}{k_B\cdot T_c}$ vs $\frac{k_B\cdot T_c}{\hbar\cdot\omega_{ln}}$ (which is often considered as an universal plot for phonon-mediated superconductors [72-75]), $C2/m\text{-SnH}_{12}$ phase falls into the lower branch (Fig. 5), where its NRTS contemplate H_3S is located [76].

It should be stressed, that in Fig. 5, a both fitting curves (red and cyan) and their 95% confidence band were not altered from ones in Fig. 4 in Ref. 76, because new fits were not performed (more details about these branches can be found in Ref. 76). It can be seen an unprecedented accuracy for the positioning of $C2/m\text{-SnH}_{12}$ phase in the lower branch. It should be noted that data on the upper branch in Fig. 5 with a very high accuracy can be described by simple elegant equation (Eq. 24 in Ref. 76):

$$\frac{2\cdot\Delta(0)}{k_B\cdot T_c} = 3.53 \cdot \left(1 + 3.53 \cdot \left(\frac{k_B\cdot T_c}{\hbar\cdot\omega_{ln}}\right)^{1.29}\right) \quad (17)$$

In Fig. 5,b we fit data for lower branch (i.e. for $\text{Pb}_{0.5}\text{Bi}_{0.5}$, $\text{Pb}_{0.75}\text{Bi}_{0.25}$, Ga, Bi, H_3S and $\text{C2}/m\text{-SnH}_{12}$) to equation [76]:

$$\frac{2\cdot\Delta(0)}{k_B\cdot T_c} = A \cdot \left(1 + 3.53 \cdot \left(\frac{k_B\cdot T_c}{\hbar\cdot\omega_{ln}}\right)^{1.29}\right) \quad (18)$$

where A is free fitting parameter. It can be seen that 95% confidence band becomes narrower in Fig. 5,b in comparison with Fig. 5,a. Deduced parameter $A = 2.86 \pm 0.05$ is practically undistinguishable from deduced $A = 2.87 \pm 0.06$ reported in Ref. 76 for this parameter.

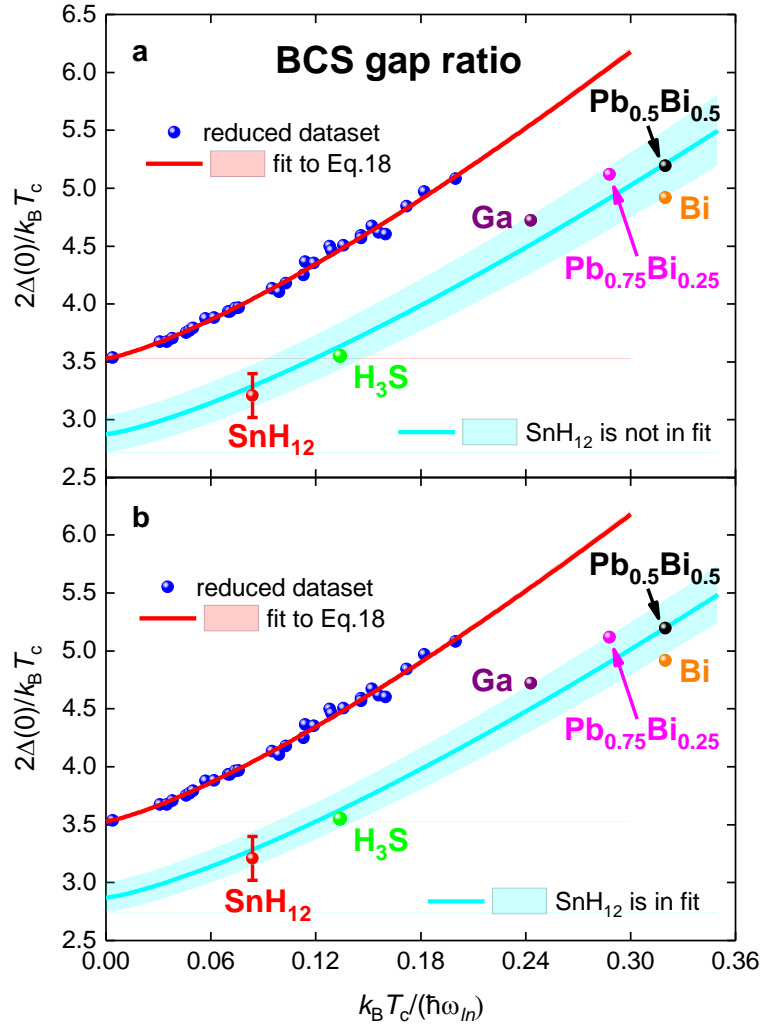


Figure 5. Full dataset of $\frac{2\cdot\Delta(0)}{k_B\cdot T_c}$ vs $\frac{k_B\cdot T_c}{\hbar\cdot\omega_{ln}}$ from Table IV of Ref. 74 and data points for highly-compressed H_3S and SnH_{12} . Fits to Eq. 17 (blue data points, red curve) and Eq. 18 (cyan curve) are shown. **a** - SnH_{12} does not include in the fit (the fit is a clone from one in Fig. 4 of Ref. 59). **b** - SnH_{12} does include in the fit. $A = 2.86 \pm 0.05$ and $R = 0.948$. 95% confidence bars are shown by a cyan shaded area.

IV. $C2/m$ -SnH₁₂ in the Uemura plot

Uemura *et al* [31,32] reported empirical discovery that all unconventional superconductors, i.e. heavy fermions, cuprates, fullerenes and, later, to this list were added the iron-based superconductors [76,78] and hydrogen-rich superconductors [42,79-81], have the ratio of the superconducting transition temperature, T_c , to the Fermi temperature, T_F , within a narrow range:

$$0.01 \lesssim \frac{T_c}{T_F} \lesssim 0.05, \quad (19)$$

while conventional superconductors have much smaller $\frac{T_c}{T_F}$ ratio:

$$\frac{T_c}{T_F} \lesssim 0.001 \quad (20)$$

It should be noted that maximal value of $\frac{T_c}{T_F} = 0.22$ is attributed Bose-Einstein condensates (BEC). Thus, further step to characterize the superconducting state in $C2/m$ -SnH₁₂ phase ($P = 190$ GPa) is to find the $\frac{T_c}{T_F}$ ratio for this compound.

The Fermi temperature can be calculated by an equation [76]:

$$T_F = \frac{\pi^2}{8 \cdot k_B} \cdot (1 + \lambda_{e-ph}) \cdot \xi^2(0) \cdot \left(\frac{\alpha \cdot k_B \cdot T_c}{\hbar} \right)^2, \quad (21)$$

where $\alpha = \frac{2 \cdot \Delta(0)}{k_B \cdot T_c}$, and λ_{e-ph} is the electron-phonon coupling constant. For calculations we utilized $\lambda_{e-ph} = 1.25$ reported by Esfahani *et al* [29] who computed by first-principles calculations several parameters for $C2/m$ -SnH₁₂ phase. The rest of parameters in Eq. 21, i.e. α , T_c , $\xi(0)$, we deduced from the analysis of $B_{c2}(T)$ data above.

In a result, calculated Fermi temperature is $T_F = 5,658 \pm 906$ K, and in the Uemura plot (Fig. 6), $C2/m$ -SnH₁₂ phase falls into unconventional superconductors band in a close proximity to YBa₂Cu₃O_{7- δ} cuprates and in the same T_c/T_F band where all NRTS counterparts are located. To date, an understanding that NRTS materials exhibit unconventional

superconductivity is becoming more acknowledged [18,83,84], because if the superconducting transition temperature, T_c , in hydrogen-rich compounds was reasonably well predicted in some (and, what is important to stress, not in all) hydrogen-rich compounds, other calculated superconducting parameters, in particular, the ground state upper critical field and the ground state London penetration depth, are different from experimental values in several times.

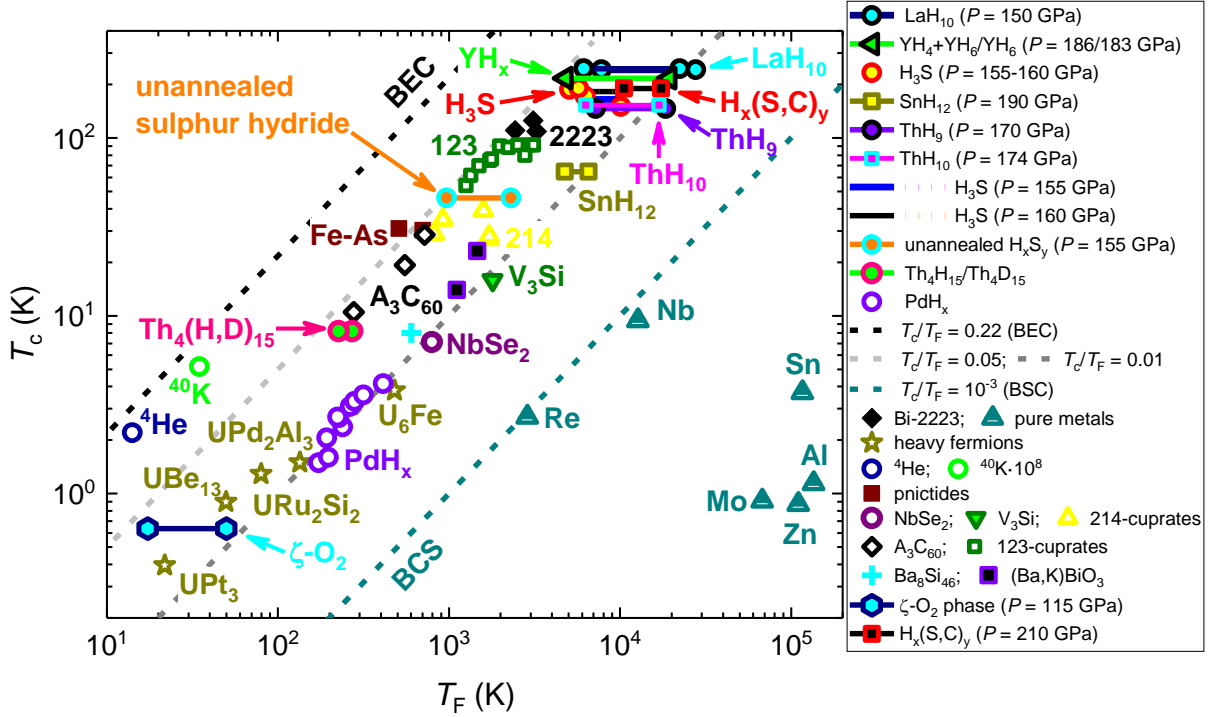


Figure 6. T_c vs T_F plot where the $C2/m$ - SnH_{12} ($P = 190$ GPa) phase is shown together with main superconducting families: elemental superconductors, heavy-fermions, pnictides, cuprates, and near-room-temperature superconductors. Reference on original data can be found in Refs. 31,32,42,77-82. Boundary lines for BCS superconductors, for Bose-Einstein condensates and for $T_c/T_F = 0.05$, 0.01 are shown.

V. Conclusions

Recently, Hong *et al* [28] discovered a new highly-compressed $C2/m$ - SnH_{12} superhydride phase which exhibits the superconducting transition temperature of $T_c = 70$ K at pressure of 190 GPa. Here we analyse the magnetoresistance data in this phase and deduce the ground state superconducting gap of $\Delta(0) = 9.15 \pm 0.51$ meV and the ratio of $2\Delta(0)/k_B T_c = 3.28 \pm 0.18$. Taking in account results of first principles calculations for this phase performed by

Esfahani *et al* [29], we calculate the Fermi temperature $T_F = 5,658 \pm 906 \text{ K}$ in this phase, which means that in the Uemura plot [31,32], this new superhydride falls to unconventional superconductors band, where all other hydrogen-rich counterparts, including near-room-temperature superconductors, are located.

Acknowledgement

The author thanks financial support provided by the Ministry of Science and Higher Education of Russia (theme “Pressure” No. AAAA-A18-118020190104-3) and by Act 211 Government of the Russian Federation, contract No. 02.A03.21.0006.

References

- [1] Satterthwaite C B and Toepke I L 1970 Superconductivity of hydrides and deuterides of thorium *Phys. Rev. Lett.* **25** 741-743
- [2] Ashcroft N W 1968 Metallic hydrogen: a high-temperature superconductor? *Phys. Rev. Lett.* **21** 1748-1749
- [3] Ashcroft N W 2004 Hydrogen dominant metallic alloys: high temperature superconductors? *Phys. Rev. Lett.* **92** 187002
- [4] Drozdov A P, Eremets M I, Troyan I A, Ksenofontov V, Shylin S I 2015 Conventional superconductivity at 203 kelvin at high pressures in the sulfur hydride system *Nature* **525** 73-76
- [5] Zhou D, *et al* 2020 Superconducting praseodymium superhydrides *Sci. Adv.* **6** eaax6849
- [6] Chen W, *et al.* 2021 High-pressure synthesis of barium superhydrides: Pseudocubic BaH₁₂ *Nature Communications* **12** 273
- [7] Drozdov A P, Eremets M I and Troyan I A 2015 Superconductivity above 100 K in PH₃ at high pressures *arXiv:1508.06224*
- [8] Matsuoka T, *et al* 2019 Superconductivity of platinum hydride *Phys. Rev. B* **99** 144511
- [9] Chen W, Semenok D V, Huang X, Shu H, Li X, Duan D, Cui T and Oganov A R 2021 High-temperature superconductivity in cerium superhydrides *arXiv:2101.01315*
- [10] Semenok D V, Kvashnin A G, Ivanova A G, Svitlyk V, Fominski V Yu, Sadakov A V, Sobolevskiy O A, Pudalov V M, Troyan I A and Oganov A R 2020 Superconductivity at 161 K in thorium hydride ThH₁₀: Synthesis and properties *Materials Today* **33** 36-44
- [11] Wang N, *et al* 2021 A low- T_c superconducting modification of Th₄H₁₅ synthesized under high pressure *Superconductor Science and Technology* **34** 034006
- [12] Einaga M, *et al* 2016 Crystal structure of the superconducting phase of sulfur hydride *Nature Physics* **12** 835-838
- [13] Mozaffari S *et al* 2019 Superconducting phase diagram of H₃S under high magnetic fields *Nat. Commun.* **10** 2522

- [14] Minkov V S, Prakapenka V B, Greenberg E, Eremets M I 2020 Boosted T_c of 166 K in superconducting D_3S synthesized from elemental sulfur and hydrogen *Angew. Chem. Int. Ed.* **59** 18970-18974
- [15] Matsumoto R, *et al.* 2020 Electrical transport measurements for superconducting sulfur hydrides using boron-doped diamond electrodes on beveled diamond anvil *Superconductor Science and Technology* **33** 124005
- [16] Huang X, *et al* 2019 High-temperature superconductivity in sulfur hydride evidenced by alternating-current magnetic susceptibility *National Science Review* **6** 713-718
- [17] Laniel D, *et al* 2020 Novel sulfur hydrides synthesized at extreme conditions *Phys. Rev. B* **102** 134109
- [18] Troyan I A, *et al.* 2021 Anomalous high-temperature superconductivity in YH_6 *Advanced Materials*, in press <https://doi.org/10.1002/adma.202006832>
- [19] Kong P P, *et al.* 2019 Superconductivity up to 243 K in yttrium hydrides under high pressure *arXiv:1909.10482*
- [20] Somayazulu M, *et al.* 2019 Evidence for superconductivity above 260 K in lanthanum superhydride at megabar pressures *Phys. Rev. Lett.* **122** 027001
- [21] Drozdov A P, *et al* 2019 Superconductivity at 250 K in lanthanum hydride under high pressures *Nature* **569** 528-531
- [22] Sakata M, *et al.* 2020 Superconductivity of lanthanum hydride synthesized using AlH_3 as a hydrogen source *Superconductor Science and Technology* **33** 114004
- [23] Hong F, *et al* 2020 Superconductivity of lanthanum superhydride investigated using the standard four-probe configuration under high pressures *Chinese Physics Letters* **37** 107401
- [24] Sun D, *et al* 2020 High-temperature superconductivity on the verge of a structural instability in lanthanum superhydride *arXiv:2010.00160*
- [25] Semenok D V, *et al* 2020 Superconductivity at 253 K in lanthanum-yttrium ternary hydrides *arXiv:2012.04787*
- [26] Ma L, *et al* 2021 Experimental observation of superconductivity at 215 K in calcium superhydride under high pressure *arXiv:2103.16282*
- [27] Li Z W, *et al* 2021 Superconductivity above 200 K observed in superhydrides of calcium *arXiv:2103.16917*
- [28] Hong F, *et al* 2021 Superconductivity at ~ 70 K in tin hydride SnH_x under high pressure *arXiv:2101.02846*
- [29] Mahdi Davari Esfahani M, *et al* 2016 Superconductivity of novel tin hydrides (Sn_nH_m) under pressure *Sci. Rep.* **6** 22873
- [30] Jones C K, Hulm J K, Chandrasekhar B S 1964 Upper critical field of solid solution alloys of the transition elements *Rev. Mod. Phys.* **36** 74-76
- [31] Uemura Y J 1997 Bose-Einstein to BCS crossover picture for high- T_c cuprates *Physica C* **282-287** 194-197
- [32] Uemura Y J 2019 Dynamic superconductivity responses in photoexcited optical conductivity and Nernst effect *Phys. Rev. Materials* **3** 104801
- [33] Talantsev E F and Stolze K 2021 Resistive transition of hydrogen-rich superconductors *Superconductor Science and Technology*, accepted, <https://doi.org/10.1088.1361-6668/abf23c>
- [34] Tinkham M 1988 Resistive transition of high-temperature superconductors *Phys. Rev. Letters* **61** 1658-1661
- [35] Hirsch J E and Marsiglio F 2021 Nonstandard superconductivity or no superconductivity in hydrides under high pressure *Phys. Rev. B* **103** 134505
- [36] Talantsev E F 2020 Advanced McMillan's equation and its application for the analysis of highly-compressed superconductors *Superconductor Science and Technology* **33** 094009

- [37] Antonova O V and Volkov A Yu 2012 Changes of microstructure and electrical resistivity of ordered Cu-40Pd (at.%) alloy under severe plastic deformation *Intermetallics* **21** 1-9
- [38] Volkov A Yu and Kazantsev 2012 Impact of the initial state on the structure and properties of the ordered CuAu alloy *The Physics of Metals and Metallography* **113** 62-71
- [39] Volkov A Yu, Novikova O S and Antonov B D 2013 The kinetics of ordering in an equiatomic CuPd alloy: A resistometric study *Journal of Alloys and Compounds* **581** 625-631
- [40] Ohta K, Kuwayama Y, Hirose K, Shimizu K and Ohishi Y 2016 Experimental determination of the electrical resistivity of iron at Earth's core conditions **534** 95-98
- [41] Deng L, Seagle C, Fei Y and Shahar A 2013 High pressure and temperature electrical resistivity of iron and implications for planetary cores *Geophysical Research Letters* **40** 33-37
- [42] Talantsev E F 2019 Classifying superconductivity in compressed H₃S *Modern Physics Letters B* **33** 1950195
- [43] Gross F, *et al.* 1986 Anomalous temperature dependence of the magnetic field penetration depth in superconducting UBe₁₃. *Z. Phys. B* **64** 175-188
- [44] Gross-Alltag F, Chandrasekhar B S, Einzel D, Hirschfeld P J and Andres K 1991 London field penetration in heavy fermion superconductors *Z. Phys. B* **82** 243-255
- [45] Talantsev E F, Mataira R C, Crump W P 2020 Classifying superconductivity in Moiré graphene superlattices *Scientific Reports* **10** 212
- [46] Talantsev E F 2020 In-plane *p*-wave coherence length in iron-based superconductors *Results in Physics* **18** 103339
- [47] Talantsev E F 2020 Classifying superconductivity in an infinite-layer nickelate Nd_{0.8}Sr_{0.2}NiO₂ *Results in Physics* **17** 103118
- [48] Kramer E J 1973 Scaling laws for flux pinning in hard superconductors *J. Appl. Phys.* **44** 1360-1370
- [49] Dew-Hughes D 1974 Flux pinning mechanisms in type II superconductors *Philosophical Magazine* **30** 293-305
- [50] Oh S, *et al* 2007 Lorentz-force dependence of the critical current for SmBCO coated conductor *J. Appl. Phys.* **102** 043904
- [51] Iida K, Hänisch J and Tarantini C 2018 Fe-based superconducting thin films on metallic substrates: Growth, characteristics, and relevant properties *Appl. Phys. Rev.* **5** 031304
- [52] Talantsev E F, Crump W P, Island J O, Xing Y, Sun Y, Wang J, Tallon J L 2017 On the origin of critical temperature enhancement in atomically thin superconductors *2D Materials* **4** 025072
- [53] Talantsev E F, Crump W P, Tallon J L 2017 Thermodynamic parameters of single- or multi-band superconductors derived from self-field critical currents *Annalen der Physik* **529** 1700197
- [54] Talantsev E F, Crump W P, Storey J G, Tallon J L 2017 London penetration depth and thermal fluctuations in the sulphur hydride 203 K superconductor *Annalen der Physik* **529** 1600390
- [55] Bardeen J, Cooper L N, and Schrieffer J R 1957 Theory of superconductivity *Phys. Rev.* **108** 1175-1204
- [56] Eliashberg G M 1960 Interactions between electrons and lattice vibrations in a superconductor *Soviet Phys. JETP* **11** 696-702
- [57] Duan D, *et. al.* 2014 Pressure-induced metallization of dense (H₂S)₂H₂ with high-*T_c* superconductivity *Scientific Reports* **4** 6968
- [58] Errea I, *et al* 2020 Quantum crystal structure in the 250-kelvin superconducting lanthanum hydride *Nature* **578** 66-69
- [59] Heil C, di Cataldo S, Bachelet G B and Boeri L 2019 Superconductivity in sodalite-like yttrium hydride clathrates *Physical Review B* **99** 220502(R)

- [60] Durajski A P 2016 Quantitative analysis of nonadiabatic effects in dense H₃S and PH₃ superconductors *Sci. Rep.* **6** 38570
- [61] Liu H, Naumov I I, Hoffmann R, Ashcroft N W and Hemley R J 2017 Potential high- T_c superconducting lanthanum and yttrium hydrides at high pressure *PNAS* **114** 6990-6995
- [62] Errea I *et al* 2015 High-pressure hydrogen sulfide from first principles: A strongly anharmonic phonon-mediated superconductor *Phys. Rev. Lett.* **114** 157004
- [63] Durajski A P and Szczyński R 2018 Structural, electronic, vibrational, and superconducting properties of hydrogenated chlorine *J. Chem. Phys.* **149** 074101
- [64] Chen J, Cui W, Shi J, Xu M, Hao J, Durajski A P, and Li Y 2019 Computational design of novel hydrogen-rich YS–H compounds *ACS Omega* **4** 14317-14323
- [65] Alarco J A, Talbot P C and Mackinnon I D R 2018 Identification of superconductivity mechanisms and prediction of new materials using Density Functional Theory (DFT) calculations *J. Phys.: Conf. Ser.* **1143** 012028
- [66] Semenok D V, Kvashnin A G, Kruglov I A, and Oganov A R 2018 Actinium hydrides AcH₁₀, AcH₁₂, and AcH₁₆ as high-temperature conventional superconductors *J. Phys. Chem. Lett.* **9** 1920-1926
- [67] Sun Y, Lv J, Xie Y, Liu H, and Ma Y 2019 Route to a superconducting phase above room temperature in electron-doped hydride compounds under high pressure *Phys. Rev. Lett.* **123** 097001
- [68] Hou P, Belli F, Bianco R, Errea I 2021 Strong anharmonic and quantum effects in $Pm\text{-}3n\text{-AlH}_3$ under high pressure: A first-principles study *arXiv*: 2102.00072
- [69] Camargo-Martínez J A, *et al* 2019 High- T_c superconductivity in H₃S: pressure effects on the superconducting critical temperature and Cooper pair distribution function *Supercond. Sci. Technol.* **32** 125013
- [70] Camargo-Martínez J A, *et al* 2020 The higher superconducting transition temperature T_c and the functional derivative of T_c with $\alpha^2F(\omega)$ for electron–phonon superconductors *J. Phys.: Condens. Matter* **32** 505901
- [71] Durajski A P, Wang C, Li Y, Szczyński R, Cho J-H 2021 Evidence of phonon-mediated superconductivity in LaH₁₀ at high pressure *Annalen der Physik* <https://doi.org/10.1002/andp.202000518>
- [72] Mitrovic B, Zarate H G, Carbotte J P 1984 The ratio $2\Delta_0/k_B T_c$ within Eliashberg theory *Phys. Rev. B* **29** 184-190
- [73] Marsiglio F and Carbotte J P 1986 Strong-coupling corrections to Bardeen-Cooper-Schrieffer ratios *Phys Rev B* **33** 6141-6146
- [74] Carbotte J P 1990 Properties of boson-exchange superconductors *Rev. Mod. Phys.* **62** 1027
- [75] Nicol E J, Carbotte J P 2015 Comparison of pressurized sulfur hydride with conventional superconductors *Phys. Rev. B* **91** 220507(R)
- [76] Talantsev E F 2020 Double-valued strong-coupling corrections to Bardeen-Cooper-Schrieffer ratios *Superconductor Science and Technology* **33** 124003
- [77] Qian T, *et al.* 2011 Absence of a holelike Fermi surface for the iron-based K_{0.8}Fe_{1.7}Se₂ superconductor revealed by angle-resolved photoemission spectroscopy *Phys. Rev. Lett.* **106** 187001
- [78] Hashimoto K, Cho K, Shibauchi T, Kasahara S, Mizukami Y, Katsumata R, Tsuruhara Y, Terashima T, Ikeda H, Tanatar M A, Kitano H, Salovich N, Giannetta R W, Walmsley P, Carrington A, Prozorov R, Matsuda Y 2012 A sharp peak of the zero-temperature penetration depth at optimal composition in BaFe₂(As_{1-x}P_x)₂ *Science* **336** 1554-1557
- [79] Talantsev E F 2020 An approach to identifying unconventional superconductivity in highly-compressed superconductors *Superconductor Science and Technology* **33** 124001

- [80] Talantsev E F 2020 Unconventional superconductivity in highly-compressed unannealed sulphur hydride *Results in Physics* **16** 102993
- [81] Talantsev E F 2019 Classifying hydrogen-rich superconductors *Materials Research Express* **6** 106002
- [82] Ye J T, *et al.* 2012 Superconducting dome in a gate-tuned band insulator *Science* **338** 1193
- [83] Dogan M and Cohen M L 2021 Anomalous behavior in high-pressure carbonaceous sulfur hydride *Physica C* 1353851 (<https://doi.org/10.1016/j.physc.2021.1353851>)
- [84] Wang T, *et al* 2021 Absence of conventional room temperature superconductivity at high pressure in carbon doped H₃S *arXiv*:2104.03710